UNSYS digital

International Journal of Robotics and Mechatronics 2018, Vol. 5, No. 1

Dynamic Analysis, Design, and Experimental Demonstration of A Gamma-Type Stirling Engine Coupled with Parabolic Dish Tracker

Muhammad I. Rashad[†], Ihab G. Adam[†], Khaled F. Shehata [‡]

[†]Department of Mechanical Power Engineeing, Faculty of Engineering, Alexandria University, Elhadara, Alexandria, Egypt

[‡]Department of Electrical Engineeing, Faculty of Engineering, Alexandria University, Elhadara, Alexandria, 21544, Egypt

Abstract—This paper presents a study of low rating gamma-type Stirling engine. Through this study, the dead volume analysis of the Stirling engine is investigated. A Simulink model is introduced to facilitate the use of the analysis with a simplified friendly graphical user interface. Based on the analysis, a realistic CAD model of a 40-Watt and 20% thermal efficiency Stirling unit is developed using Solidworks. Using the Finite Element Analysis (FEA) simulations, the motion and dynamic analysis are carried out for the proposed design to investigate the effects of inertia and friction on the engine performance. After that, the parabolic dish tracking system is introduced and the two axes system design is discussed in details. Finally, the integrated system of the Stirling unit with the tracker is manufactured and established at the Faculty of Engineering, Alexandria University, Alexandria, Egypt. The unit is fully functional and was operated during summer days.

Keywords— Stirling engine, solar energy, dynamic analysis, parabolic dish

Copyright©2017. Published by UNSYSdigital. All rights reserved.
DOI: https://doi.org/10.21535/ijrm.v5i1.986

I. INTRODUCTION

NOWADAYS, the continuous increase in worldwide energy demand and the increase in consumption of fossil fuels, as well as global warming caused by fossil fuels constitute a serious problem that needs to be solved. The reduction of air pollution and greenhouse effect gases, and the protection of water sources are the main advantages of solar energy.

The Stirling engines are thermally regenerative, simple in construction and manufacturing, relatively quiet, safe in operation. As an externally heated engine, the Stirling engine has the advantage of being able to efficiently run on various waste heat sources especially the vast amount of waste heat emitted from industrial processes and renewable thermal energy sources to generate electrical power [1].

These days, solar dish Stirling power generators are classified as one of the the most efficient solar approaches by exceeding the efficiency of any other solar conversion technology [2]. Each parabolic dish/Stirling system is considered a stand-alone power generator which allows its deployment individually for off-grid applications and their installations. For this reason, this technology seems to be the most promising to be applied in remote areas with limited or no access to electrical grid [3,4].

Lovegrove et al. [5] developed a new 500m^2 parabolic dish prototype of a design optimized for fabrication. The construction of the prototype has successfully proven a range of novel design features including the use of the mirror panels to be a part of the structure itself. Nepveu et al. [6] presented a global thermal model of the 10kW Eurodish dish/Stirling unit. Wu et al. [7] evaluated the thermal-electric conversion performance of parabolic dish/AMTEC. The efficiency reached 20.6% with an output power of 18.54 kW.

Stirling engines are mechanically arranged into three types, which are alpha, beta and gamma. Cheng and Yang [8] reviewed the major differences between these three types and investigated their relative performance aiming for the optimization of geometrical parameters. For all of the three configurations, the cycle is thermodynamically similar. In alpha Stirling engine type, hot and cold pistons are mounted in separate cylinders placed on each side of the regenerator. The V arrangement and the yoke drive (Ross linkage) are often applied to this type of engine. The beta Stirling engine type consists of power piston and displacer incorporated in the same cylinder. One mechanical disadvantage is that a drive rod from the displacer extends through the piston. On the other hand, higher compression, efficiency, and power can be obtained due to lower dead volume. In gamma Stirling engine type, the power piston and displacer are located in two separate spaces. The power piston, which is located at the cold side of the chamber, compresses or expands the gas being pushed into the cylinder. This configuration of the engine is mechanically more efficient than the others [9].

The regenerator is a key component of the engine [10], as it acts like a thermal storage. The working gas transfers from the

Corresponding author: Muhammad I. Rashad
(e-mail: m.rashad_88@yahoo.com)

This paper was submitted on Oct 23, 2017; and accepted on Oct 23, 2017.

hot chamber through the regenerator to the cold chamber in the first half of the engine cycle. The regenerator, which contains a filling porous and highly conductive material, absorbs the heat from the hot gas. The working gas is sent back through the regenerator from the cold side to the hot side. The cold gas absorbs the stored heat from the regenerator filling. This minimizes the amount of energy that needs to be added to the heater. On the other hand, the gas leaving the regenerator loses a part of its temperature and arrives at the cooler at a lower temperature. This then minimizes the heat rejection [11]. Developers who do not have efficient-regenerator fabrication technology should take into account the regenerator effectiveness, and then an analysis with imperfect regeneration should be made [12].

The contributions of this paper are

1) The Simulink model that can easily be used to investigate and design of any type of Stirling engine, with the simplified Graphical User Interface (GUI) is considered to be a simple preliminary step for the design and fabrication.
2) Dynamic analysis that shows the effect of the friction and inertia on the engine performance is presented.
3) The design and fabrication of both the Stirling engine and the prabolic dish tracking are presented, in conjunction with all the notes that explain why a Stirling engine may practically fail to start.

Section II describes the Stirling engine analysis and the effect of dead volumes on the engine performance. Dead volume analysis is the analysis consisdered through this paper. This is followed by the development of a Simulink model that simplifies and facilitate the use of the given analysis. Section III discusses the Computer Aided Design (CAD) modelling of a realistic 40Watt gamma-type Stirling engine. The CAD model is discussed in details giving all the notes required for the fabrication phase. Section IV contains the motion study using Finite Element Analysis (FEA) to investigate the effect of the friction and inertia of the mechanism on the engine performance. Section V includes the experimental demonstration of the Stirling engine unit integrated with the solar tracker. The manufacturing process of each component is explained and the experimentally obtained results are presented. Finally section VI contains the conclusion and summarizes the paper.

II. Stirling Engine Analysis

The modelling of Stirling engine can substantially contribute to the development of this technology and help the understanding of the fundamental processes of the real cycle for further improvements.

Schmidt's analysis [13] is known as the first order method to predict engine power, often called isothermal analysis. It is an analytical approach based on isothermal working space and sinusoidal volume changes. The conventional analysis of Stirling engine usually assume the absence of dead volumes especially for the regenerator, in addition to the assumption of perfect regenerator with 100% efficiency which is practically impossible. This causes great deviation in the theoretical and practical values of the engine which can be very misleading especially for researchers who are aiming to develop a working Stirling engine for experimental purposes. On the other hand, the dead volume analysis tries to make imperfect realization for Stirling engine, as it contains dead volumes and regenerator whose efficiency actually varies from 0% to 99%.

A. *Dead volume analysis*

This section presents a brief discussion regarding Stirling engine dead volume analysis, considering the analysis that was published by Kongtragool and Wongwises [12]. The dead volume analysis is considered as a theoretical investigation on the thermodynamical analysis of a Stirling engine. An isothermal model is developed for an imperfect regeneration Stirling engine with dead volumes of hot space, cold space and regenerator that the regenerator effective temperature is an arithmetic mean of the heater and cooler temperature.

The following section states the main parameters and driving equations of the analysis to investigate the engine thermal efficiency and overall performance.

The main parameters of the analysis are listed in Table 1. T1, T1', T3 and T3' are the temperatures of the cycle state points as stated in Figure 1.

Table 1 Analysis main parameters

m	Total mass of fluid inside the engine (kg)
P	Absolute pressure (N/m²)
Q_A	Total heat added from an external source (J)
Q_R	Heat rejected to the outside through the cycle(J)
W_{net}	Net engine power (J)
R	Gas constant (J / kg K)
C_V	Specific heat at constant volume (J / kg.K)
E	Efficiency of the regenerator
E_t	Thermal efficiency of the Stirling engine
K	Factor defined by equation (5)
ɣ	Specific heat (J/kg.K)
V_T	Total volume of working gas in the engine (m^3)
V_{dh}	Dead hot volume (heater, links, cylinder) (m^3)
V_{dc}	Dead cold volume (cooler, links, cylinder) (m^3)
V_{dr}	Dead volume of the regenerator (m^3)
V_P	Volume swept by the working piston (m^3)
V_D	Volume swept by the working displacer (m^3)
k_{dh}	V_{dh}/V_{dt}
k_{dr}	V_{dr}/V_{dt}
k_{dc}	V_{dc}/V_{dt}
k_{dt}	V_{dt}/V_T
k_{dDP}	$V_{dt}/(V_D + V_P)$
T3	Temperature of working gas in the hot space (K)
T3'	Temperature of working gas leaving the regenerator (K)
T1	Temperature of the working gas in the cold space (K)
T1'	Temperature of working gas at the inlet of the regenerator (K)
TR	Temperature of working gas contained in the regenerator (K)
Tc	Cooler temperature (K)
Th	Heater temperature (K)

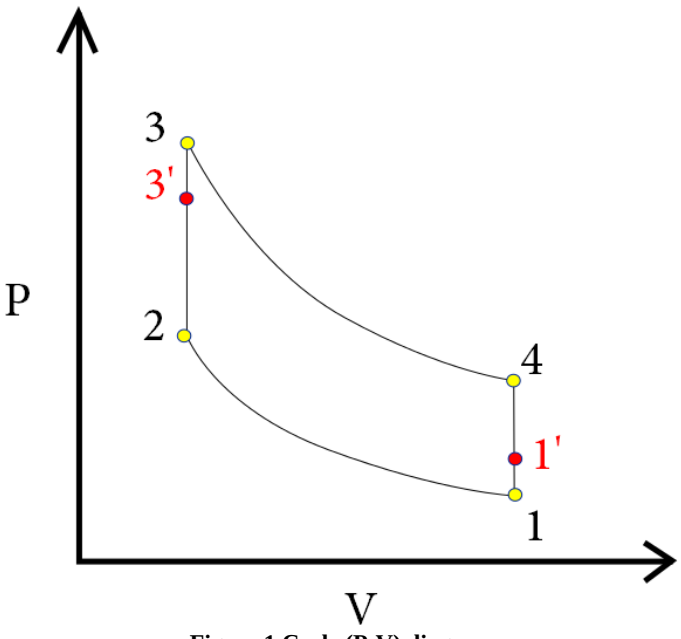

Figure 1 Cycle (P-V) diagram

Based on the previous table the driving equations can be listed as the following [12]:

1) Dead volumes

$$V_{dt} = V_{dh} + V_{dr} + V_{dc} = (k_{dh} + k_{dr} + k_{dc})V_{dt} \quad (1)$$

$$V_{dt} = k_{dt}\,V_T = k_{dt}\,(V_{dt} + V_D + V_P) \quad (2)$$

$$V_{dt} = k_{dDP}\,(V_D + V_P) \quad (3)$$

2) Absolute pressure

$$P = \frac{mR}{\frac{V_h}{T3} + \frac{V_{dh}}{T3} + \frac{V_{dr}}{Tr} + \frac{V_{dc}}{T1} + \frac{V_c}{T1}} = \frac{mR}{\frac{V_h}{T3} + K + \frac{V_c}{T1}} \quad (4)$$

3) The factor (K)

$$K = \left(\frac{k\,dh}{T3} + \frac{2k\,dr}{T3 + T1} + \frac{k\,dc}{T1}\right) V_{dt} \quad (5)$$

4) Isothermal compression process

$$Q_{1-2} = mRT_1\ \ln\left(\frac{V_D + KT1}{V_D + V_P + KT1}\right) \quad (6)$$

5) Isochoric heating process

$$Q_{3-3'} = (1-e)mc_V\,(T\,3 - T\,1) \quad (7)$$

6) Isothermal expansion process

$$Q_{3-4} = mRT_3\ ln\,(\frac{V_D + V_P + KT3}{V_D + KT3}) \quad (8)$$

7) Isochoric cooling process

$$Q_{4-1'} = -(1-e)mc_V\,(T\,3 - T\,1) \quad (9)$$

8) Total heat added

$$\mathrm{Q_A} = \mathrm{mc_V}\left((1-\mathrm{e})(\mathrm{T3}-\mathrm{T1}) + (\mathrm{K}-1)\mathrm{T3}\ln\left(\frac{\mathrm{V_D}+\mathrm{V_P}+\mathrm{KT3}}{\mathrm{V_D}+\mathrm{KT3}}\right)\right) \quad (10)$$

9) Total heat rejected

$$\mathrm{Q_R} = \mathrm{mc_V}\left((1-\mathrm{e})(\mathrm{T3}-\mathrm{T1}) + (\mathrm{K}-1)\mathrm{T3}\ln\left(\frac{\mathrm{V_D}+\mathrm{V_P}+\mathrm{KT1}}{\mathrm{V_D}+\mathrm{KT1}}\right)\right) \quad (11)$$

10) Net work

$$\mathrm{W_{net}} = \mathrm{mRT3}\ln\left(\left(\frac{\mathrm{V_D}+\mathrm{V_P}+\mathrm{KT3}}{\mathrm{V_D}+\mathrm{KT3}}\right) - \mathrm{T1}\ln\left(\frac{\mathrm{V_D}+\mathrm{V_P}+k\mathrm{T1}}{\mathrm{V_D}+k\mathrm{T1}}\right)\right) \quad (12)$$

11) Mean effective pressure

$$\mathrm{P_m} = \left(\frac{(\mathrm{P_3}+\mathrm{P_2})\mathrm{V_3}}{\mathrm{V_1}-\mathrm{V_2}}\right)\ln\left(\frac{\mathrm{V_1}}{\mathrm{V_2}}\right) \quad (13)$$

12) Thermal efficiency

$$E_t = \frac{mRT3\ln\left(\left(\frac{V_D+V_P+KT3}{V_D+KT3}\right) - T1\ln\left(\frac{V_D+V_P+KT1}{V_D+KT1}\right)\right)}{T3\ln\left(\frac{V_D+V_P+KT3}{V_D+KT3}\right) + (T3-T1)\frac{(1-e)}{(K-1)}} \quad (14)$$

B. Simulink model

In order to simplify the use of the previous analysis and to deal with it through a user friendly interface a Simulink [14] model was built as illustrated in Figure 2. This model represents a simple tool that can be used to design or investigate the Stirling engine performance knowing the general operating conditions.

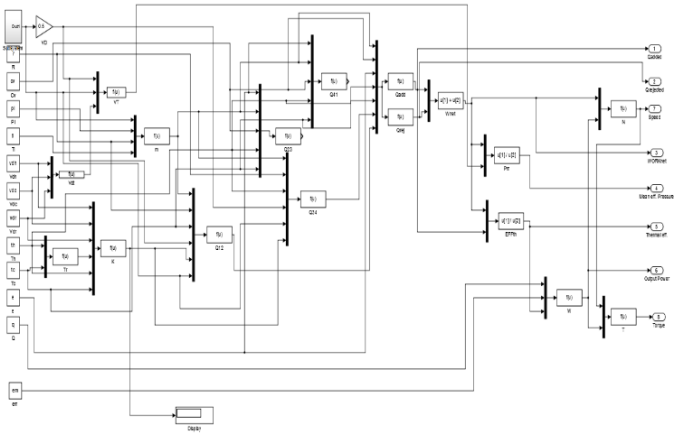

Figure 2 Simulink schematic

The input window of the developed model is illustrated in Figure 3. First of all, it includes a drop down menu to choose the working fluid. This is followed by blank spaces of the different input parameters to be filled by the user.

The inputs are divided into three main groups. The first group at points (1), (3), (4) and (12) contains the initial operating conditions parameters. The second group at spaces (8), (9) and (10) represents the steady state operating conditions. Finally, the third group, which includes the spaces at (2), (5), (6), (7) and (11), contains mainly the design parameters. Hence, it is clear that the performance of the stirling is strongly dependent on geometrical and physical parameters such as dimensions, heat source temperatures and regenerator characteristics.

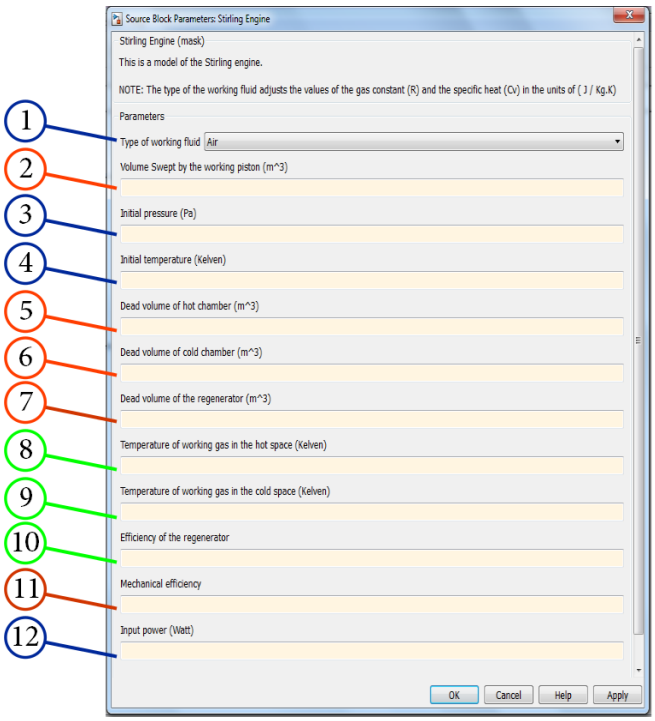

Figure 3 Simulink model user input window

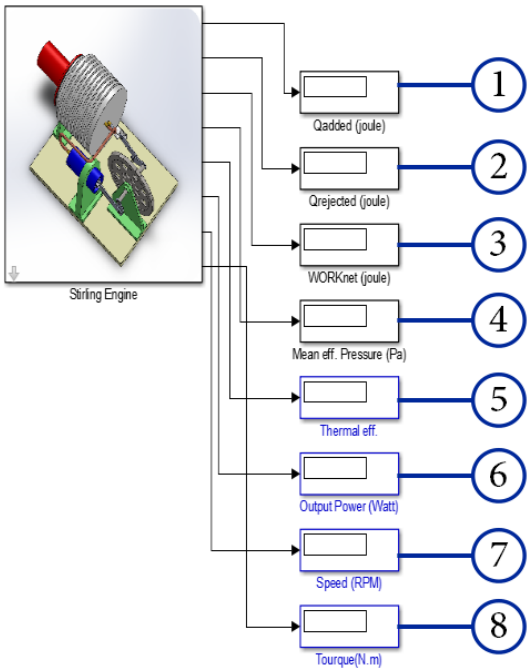

Figure 4 Simulink model output screen

Figure 4 shows the output screen. It displays eight results starting at point (1) with the heat added during a single cycle, followed by the corresponding values for the heat rejected and the work at points (2) and (3) respectively. The mean effective pressure, thermal efficiency, output power, rotational speed and net torque will be displayed at points (4), (5), (6), (7) and (8) respectively. As shown above, the model is straightforward and very easy to use. It also does not require from the user to have any programming background.

C. *Simulink results*

Throughout this part the Simulink results are illustrated and the effect of the dead volumes will be discussed.

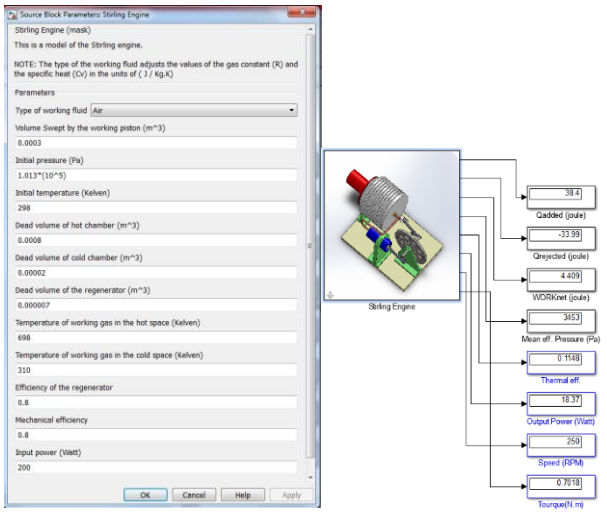

Figure 5 Engine with reasonable inputs

In Figure 5, reasonable input values were used and as shown the output values indicated that the engine will have a thermal efficiency of around 11.5%, an operating speed of 250 rpm and will be rated at 18.4 Watts.

In order to check the effect of dead volumes on engine performance zero values of dead volumes will be applied to the same engine analyzed in the previous figure. The new results are shown in Figure 6.

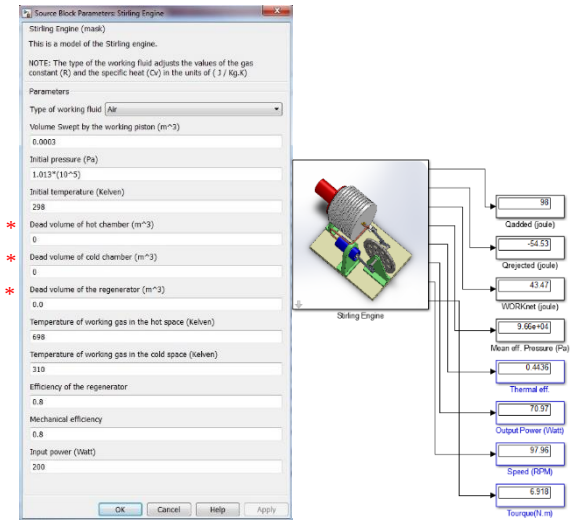

Figure 6 Engine with zero dead volume

It is important to mention that having a Stirling engine with zero dead volumes is practically impossible. For example, the regenerator will always have a dead volume. An undesired expansion will always happen in this volume causing power loss. The clearance between the displacer and the walls of the hot chamber will always be there and there is no way to eliminate it. Finally, other dead volumes will be added as a result of some material and fabrication constrains. Hence this is

a theoretical assumption and the main challenge for designers and developers is to keep the dead volumes as minimum as possible.

On comparing the previous results, the effect of the dead volumes appears very significant as the expected thermal efficiency of the engine increased by nearly 4 times from 11.5% to more than 44%. This proves that the engine performance is highly sensitive to the change of the dead volumes. It is also obvious that the dead volumes greatly affect the output torque of the engine as it increased by nearly 10 times from 0.7011 N·m to 6.918 N·m.

III. CAD Modeling for The Proposed Engine

This section illustrates the concept design of the proposed gamma-type engine. The CAD model was developed on Solidworks and is mainly designed to be used for both the dynamic analysis that is carried out through the following pages using advanced FEA motion study simulation, and the manufacturing requirements in the experimental phase.

A basic CAD model was developed based on the design data illustrated in Figure 7. The engine is expected to have a thermal efficiency of around 20%, achieving a top speed of 180 rpm with total output power of 40 Watts. One of the major values that must be taken in consideration during the design process is the amount of heat rejected, as the engine is expected to reject about 210 Watts. Hence, a relatively larger surface area is needed to successfully reject this amount of heat.

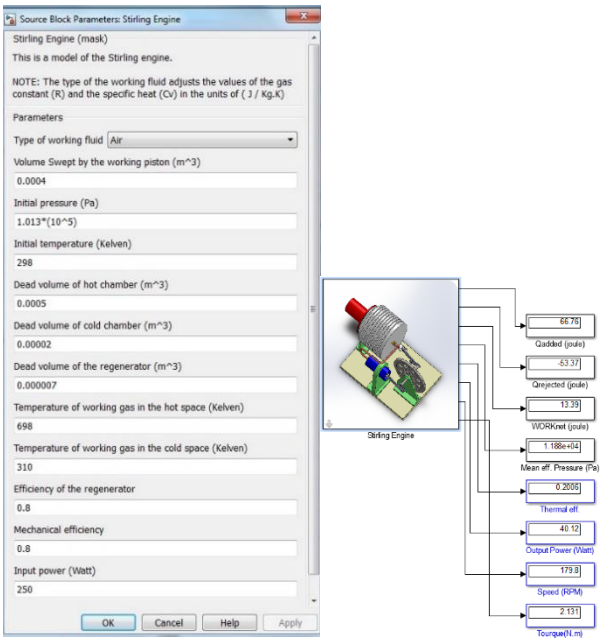

Figure 7 Design data for CAD model design

The CAD model, described in Figure 8, contains the heat receiver found at the point denoted by (1) in the figure. The heat receiver is placed at the focal point of the parabolic dish. To achieve the best results, the receiver should be coated with dark black color. It is also preferable to make it of a thin and highly conductive material in order to increase the response of the engine to the heat input. To allow perfect quick contraction of the air behind the displacer, the rest of the hot chamber at the point denoted by (4) in Figure 8, should be designed to reject as much heat as possible. To overcome some manufacturing constrains, the shown aluminum part was designed with relatively large dimensions as indicated. It would be better to have a smaller one if precise fabrication facilities are provided. In the design, the hot chamber is divided into two main parts. This is of great importance to have thermal insulation at the point denoted by (3) in Figure 8 in order to avoid the dissipation of heat from the receiver to the heat think.

The cold chamber, denoted at (2) in Figure 8, is located at an optimum distance from the hot chamber. It should be located as away from the heating source but in the same time not so far from the hot chamber, to avoid the increase of the dead volume in the regenerator. The copper tube, denoted by (5) in Figure 8, connects the two chambers and represents the regenerator.

As mentioned later in this paper, the flywheel, which is introduced at point (6) of Figure 8, plays an important role in engine smooth operation. It should be noted that a small flywheel will cause distorted motion and a heavy flywheel can prevent the engine from starting. The plate at denoted by (7) in Figure 8, is used to fix all of the components in the required position relative to each other.

The hollow aluminum displacer denoted by (10) is used to move the air between the cold and hot spaces. This is performed through the 3mm clearance denoted by (9) between the displacer and the hot chamber`s inside wall. A small clearance may cause power losses, as a result of high pumping losses that will occur especially when the engine is running at high speed.

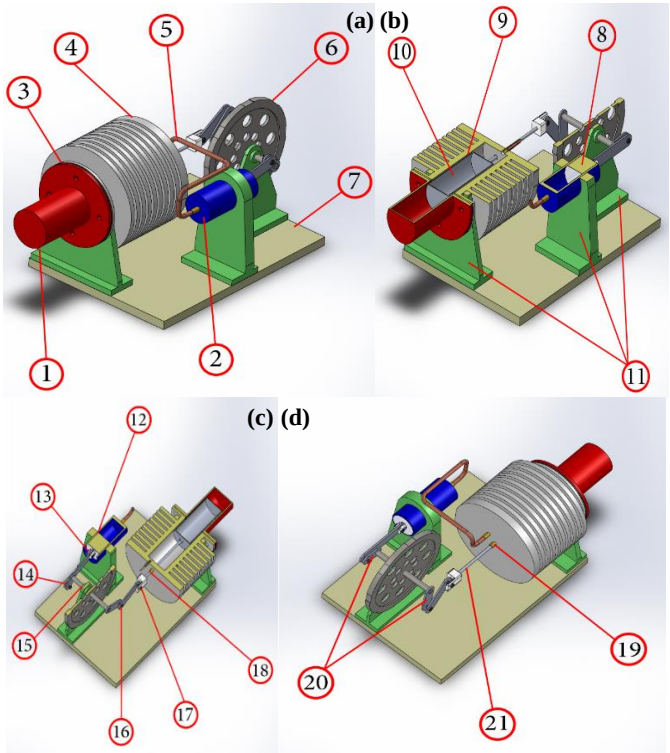

Figure 8 (a) and (d) Engine main components; (b) and (c) Sectional views of the engine

It is recommended that the piston, which is located at point (8) in the figure, is made of a light weight material. The supports

at denoted at (11) are mainly used to fix the engine components to the base.

The cranks and connecting rods at (20) of both the piston and the displacer are made of aluminum. To fulfill the heat cycle requirements both cranks are aligned perpendicular to each other. At point (21) of the figure the stainless steel 5mm displacer rod is reciprocating through the copper gland found at point (19) in the same figure. This point is considered the major leakage position in the engine and hence precise manufacturing and grinding should be applied.

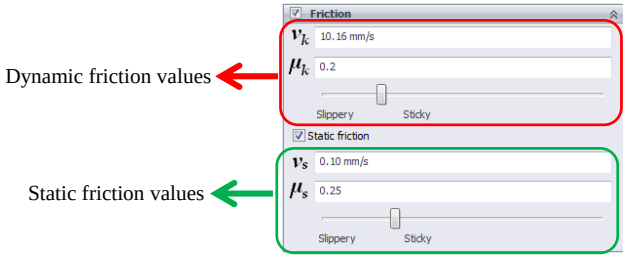

Figure 9 Friction input screen

For dynamic analysis purposes, friction is applied at the contact surfaces between any two moving parts. Dynamic and static frictions are applied according to the values illustrated in Figure 9. In this figure, greasy contact with metallic surface is assumed. v_k and μ_k are the dynamic friction velocity and dynamic friction coefficient respectively. v_s and μ_s are the static friction velocity and static friction coefficient respectively.

The contact surfaces are located in Figure 8(c) as the following:

- At (12) between the piston and cylinder.
- Between the flywheel and the flywheel support at (15).
- At (18) between the displacer rod and the copper gland.
- The friction over the pins at (13), (14), (16) and (17).

IV. Finite Element Analysis (FEA) Motion Study Simulation

This section describes in details the dynamic behavior of the Stirling engine mechanism. It demonstrates the effects of friction and inertia of the mechanism while operating at different speed ranges.

The simulation was performed using Solidworks FEA (Finite Element Analysis) motion study and using the same CAD model that was developed earlier.

A. Adding variable speed motor

The motion analysis starts by adding a virtual motor to drive the Stirling engine, the motor is set to operate for 40 seconds. It rotates counter-clockwise as illustrated in Figure 10. The motor accelerates to achieve its highest rotational speed of 1350 deg/sec (225 rpm approximately) after 20 seconds. It then decelerates till it comes to complete stop at the end of the 40 seconds.

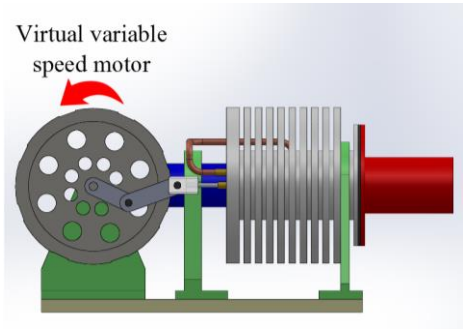

Figure 10 The virtual motor rotation direction

It is important to keep in mind that through this virtual test the motor is working against the friction and the inertia of the mechanism. Hence the readings that are discussed in the following section can give a clear overview of both characteristics, which will consequently help in predicting their influence on the engine performance.

B. Dynamic analysis results

Through the following illustrations, the red line will represent the operating condition of the proposed engine. This condition is at a rotational speed of 1080 deg/sec (180 rpm). The 180 rpm is the value that was obtained from the Simulink model earlier from Figure 7.

In Figure 11, the rotational speed in deg/sec versus the time is illustrated. It is notable that the engine will reach a value of 1080 deg/sec (180rpm) at the red line after nearly 11 seconds.

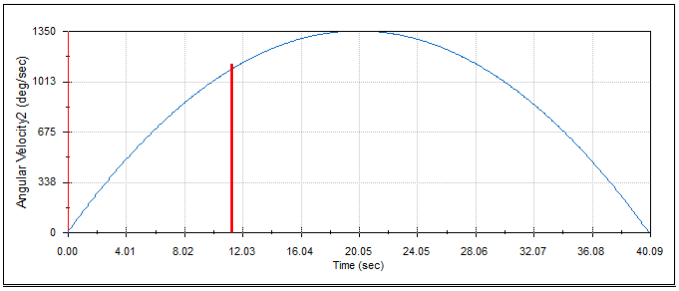

Figure 11 Rotational speed vs. time

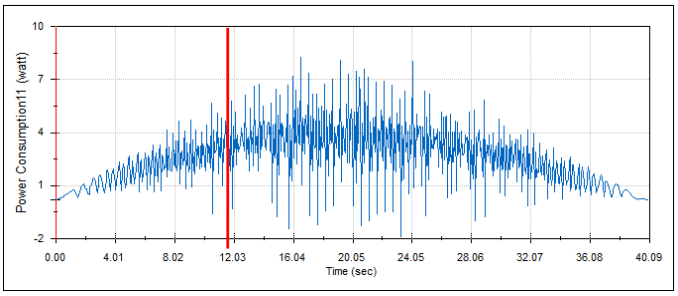

Figure 12 Power consumption vs. time

The power consumption readings over the 40 seconds are illustrated in Figure 12. It is obvious that there will be about 8.5Watt losses due to friction and inertia when the engine is operating at nearly 1350 deg/sec (225rpm). According to the plot the proposed design is expected to have around 5.5 Watt (indicated by the red line) as mechanical losses which are

equivalent to 13.75% of the total 40 Watt expected output power. This means that the engine`s mechanical efficiency will be about 86.25%, which is considered a normal value for the small size engines due to the following reasons:

1) The small contact areas between the components which are in direct contact.
2) The small and light parts used in the engine mechanism. For example, the crank and connecting rod are made of aluminum with extreme light weight.
3) The thermoplastic (nylon 66) piston and the hollow aluminum displacer.
4) The low operating speed range.

As seen in Figure 12, the fluctuation in the power consumed is due to the presence of the flywheel, which stores and discharges the energy periodically.

Figure 13 demonstrates the torque needed by the electric motor to overcome the resistance of the Stirling mechanism. As shown, the maximum torque required is about 360 N·mm (0.36 N·m). This means that the engine must produce higher torque than 0.36 N·m in order to start rotation, which is the case in the proposed engine as the theoretical value of the torque developed is equal to 2.13 N·m as was illustrated at the bottom right in Figure 7.

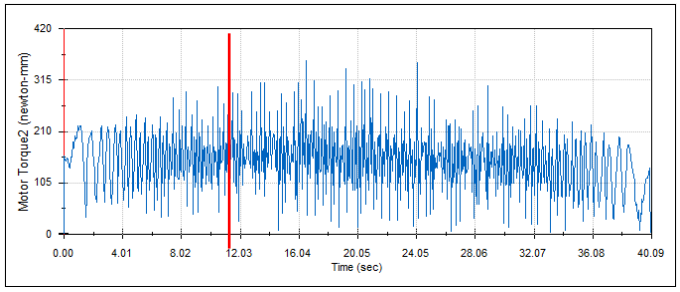

Figure 13 The motor torque vs. time

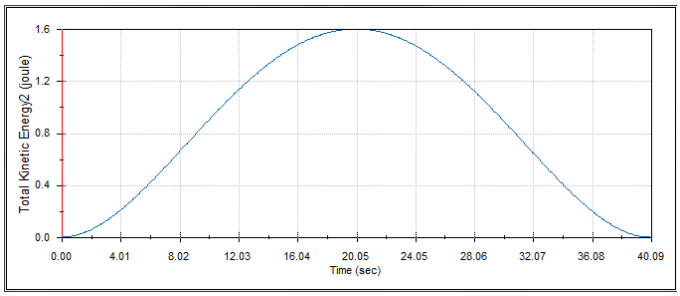

Figure 14 The total kinetic energy of the fly wheel vs. time

The flywheel is of great importance in any engine to achieve a smooth, continuous and balanced operation. This importance increases significantly in engines with low number of acting cylinders such as the Stirling engine. The smooth curve of total kinetic energy of the flywheel is illustrated in Figure 14. It is an indication for an accepted design and indicates also smooth operation over the time interval.

The reciprocating piston located in the cold chamber in gamma-type engine, is considered one of the major friction loss sources. The main reason is the relatively large contact area between the piston and the cylinder. From Figure 15 it can be deduced that, the engine piston will move with linear velocity of 460 mm/sec (4.6 m/sec), which will result in significant friction losses.

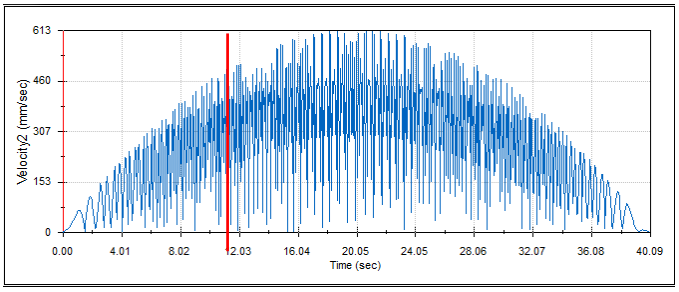

Figure 15 Piston linear velocity vs. time

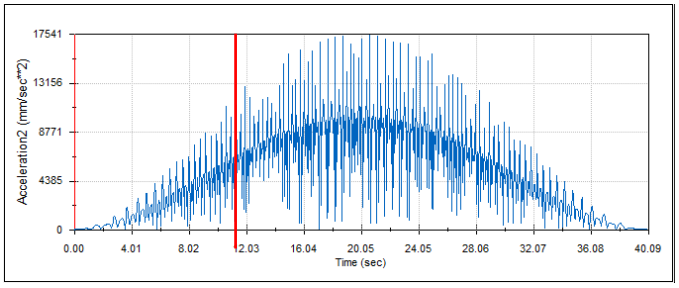

Figure 16 Piston acceleration

The acceleration of the piston is illustrated in Figure 16. All of the previous figures give a general overview of the system dynamic performance at different speeds. It is important to mention that, providing sufficient lubrication is of great importance. As the engine may fail to start under poor lubricating conditions.

V. Expermintal Demonstration

Throughout the following section, the manufacturing and development of the Stirling engine and the parabolic dish tracker proto-types are discussed in details.

It is important to mention that all the shown measurments and the results were between 11:00 AM and 4:00 PM during the month of July, the setup was established at the Faculty of Engineering, Alexandria University, Alexandria, Egypt.

A. The Stirling engine proto-type

Based on the previous design, the Stirling engine demonstrated in Figure 17 and Figure 18 was manufactured to meet the required specifications and ratings.

Aluminum and stainless steel are the major materials that were used in most of the parts. Conventional turning and machining were used in the fabrications. In order to avoid leakage all the expected positions of leakage were tightly sealed. The sealing was performed using thermal silicon. To avoid any leakage between the piston and the cylinder, precise grinding was carried out for the piston.

The conventional regenerator types adopted in Stirling engines are either wire mesh or random fiber [13]. Fillings of thin wire metallic material was added at the back of the displacer space. This increases the efficiency of the regeneration process significantly as a result of increasing the

total contact surface area. This also minimize the total dead volume of the Stirling engine and consequently increasing the thermal efficiency.

Figure 17 Stirling model view (a).

Figure 18 Stirling model view (b)

The thin wires were also used inside the regenerator copper tube for the same mentioned purposes.

B. Parabolic dish tracker proto-type

The parabolic solar dish is one of the important methods that uses the sun heat as a source of generating electricity. This is performed by concentrating the sun heat at the desired position. For Stirling engines, the solar dish tracks the sun direction to focus the heat on the receiver, which drives a Stirling engine-generator unit. Prototypes of solar tracking systems [15-19] were built to achieve this cause.

The parabolic dish systems consists of a parabolic reflector in the form of a dish with a supporting structure. For the Stirling engine to receive solar radiation, it is mounted at the focal point of the parabolic dish. To generate electrical energy, a generator is coupled to the Stirling engine. Throughout the day, the solar parabolic dish is directed toward the sun automatically using tracking control system.

The good solar dish tracking features were stated by Hafez et al. [20] as the following:

1) Reasonable weight.
2) Hardness against deflection and wind load.
3) Durability against moisture and temperature changes (the highest and the lowest temperature at different weather conditions and locations).
4) Parts must be flexible and low in cost.
5) Effective reflecting materials.
6) Long lifetime.

Figure 19 shows the two axes tracking system design. It was designed to hold a 1.2m wide steel dish. The mechanism is able to rotate the dish 120° about each axis, in order to achieve this, two linear actuators are used, each of 60cm stroke. The linear actuator is driven by a 12Volt DC motor. The motor is coupled with a power screw through an internal gearbox. The gearbox reduces the velocity to achieve high force. The high force which is achieved at minimum speed is optimum for the tracking application. Each actuator can withstand a static load of around 150 kgf.

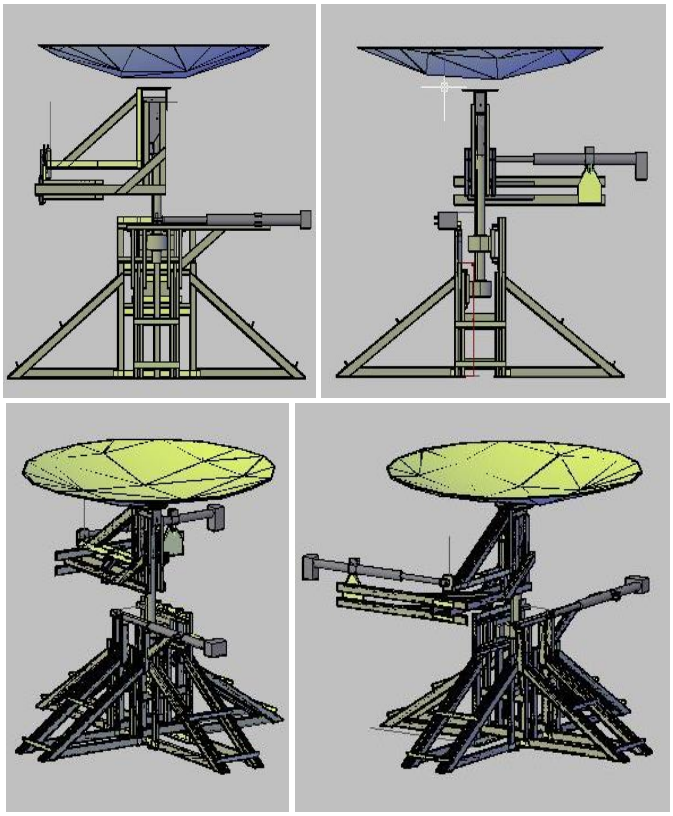

Figure 19 Parabolic dish tracker design

The structure was built using aluminum sections. Despite the relatively high cost of aluminum if compared to iron, it has a superior advantages regarding its machining cost and the ease of handling due to its light weight. With minimum needs of installation preparation and minimum maintenance requirements, aluminum is considered a perfect match for outdoor applications. Counter weights are used to balance the dish and minimize the load over the actuators.

The tracking system depends on LDR sensors in tracing the sun. The LDR sensors resistance changes according to light intensity. Using four sensors, each is enclosed inside a convenient case that allows the entrance of light when it is only perpendicular to the casing surface. Depending on the sensors signals, along with a simple AVR ATmega32 micro-controller the motion of the actuators can be fully controlled.

In the proposed model a 1.2m diameter steel dish is used as illustrated in Figure 20. In order to avoid any distortion of light, the dish was sanded using extra fine sand paper. The sand paper grade was P3000 (grades are according to the Federation of European producers of abrasives). Afterwards thin solar film strips are used as the main reflecting material.

During the summer days, the ranges of temperature achieved at the focal point were from 300 C to 350 C. Heat transfer rate was calculated by attaching a small metallic vessel of water at the focal point. Knowing the initial temperature, the amount of water and the time taken by the water to boil the actual heat transfer rate ranged from 200 Watt to 300 Watt. The variation was a result of several distortions and loss parameters such as the wind and clouds.

The reflector average efficiency ranged from 25% to 30%, which is considerably low due to the poor reflective material used. However the final output of 200 Watt to 300 Watt will be enough to run the 40Watt proposed Stirling engine.

Finally the dish is attached to the mechanism as shown in Figure 21. The mechanism was stable and there was no need for other fixations to hold the tracker to the ground. However extra fixation may be considered to withstand tough windy conditions in winter.

C. Coupling the engine with the parabolic dish tracker

As demonstrated in Figure 22, the Stirling unit is coupled with the tracker using aluminum disc and 3 steel rods. It is important to consider the size of the rods to avoid any undesired shadings.

After having the fixed Stirling engine in place, the counter weight was calibrated and the actuators testing took place. The sensors also needed a lot of calibration in order to achieve the desired results.

Figure 23 shows the Stirling engine unit operating at 3:00 PM in July. The engine rotational speed exceeded 180 rpm at no load.

Figure 20 The 1.2 m wide dish used

Figure 21 Attaching the dish to the tracker

Figure 22 Calibration of counter weight and actuator testing

Figure 23 The Stirling is operating at 3:00 pm in July

VI. Conclusions

This work presents an investigation of low power gamma-type Stirling engine and parabolic dish tracker. The study starts with the Stirling engine analysis followed by the development of the Simulink model. The analysis showed that the thermal efficiency of the engine is dependent on the values of dead volumes. As the dead volumes increases the thermal efficiency decreases. It was also found that the output net torque is the most affected parameter with the changes in dead volumes.

After that a CAD model design of a 40Watt Stirling engine and theoretical thermal effeciency of 20% was introduced. The design was discussed in details and was developed for the purposes of motion analysis and fabrication.

Motion study was performed using the Finite Element Analysis (FEA) Solidworks motion analysis. It was found that the power losses due to friction is directly proportional to the rotational speed. The value of the torque needed for the proposed engine to start up was found to be 0.36 N·m. The engine was found to consume about 5.5 Watt to overcome the friction losses at 180 rpm rotational speed. The maximum consumption was found to be 8.5 Watt at a maximum speed of about 225 rpm.

Afterwards the tracker was introduced. The two axes tracking system was designed to hold a 1.2m wide steel dish. The mechanism was able to rotate the dish 120° about each axis. In order to achieve the desired motion, two linear actuators were used each of 60cm stroke. The actuator consisted of a 12Volt DC motor with a rated 150kgf static load. The Stirling unit and the parabolic dish tracker were locally fabricated. The manufacturing procedures were discussed.

During summer days, the ranges of temperature at the focal point were found to be from 300 C to 350 C. The heat rate delivered at the focal point was calculated to be 200 Watt to 300 Watt. It was observed that the values were greatly affected by wind and clouds. The dish reflective efficiency was found to be in the range of 25% to 30%. The Striling unit after being integrated with the tracker achieved angular speed ranging from 120 rpm to 200 rpm depending on the time and conditions of operation.

Finally, further experimental measurements should be carried out for longer time at different seasons. Designs with different dimensions and specifications should be investigated.

Acknowledgment

The authors of this work gratefully acknowledge Mohamed Hegazy, Hossam Alaa Eldin and Ahmed Abdelghany for their mechanical assistance. The authors would also like to acknowledge valuable discussions with Ragy Samy and Hassan Zayton from the Electrical Engineering department.

References

[1] Allan J. Organ, The Air Engine: Stirling cycle power for a sustainable future. Elsevier, 2007.

[2] J. Khan and M. H. Arsalan, “Solar power technologies for sustainable electricity generation - A review,” Renewable and Sustainable Energy Reviews, vol. 55. pp. 414–425, Mar-2016.

[3] A. Poullikkas, G. Kourtis, and I. Hadjipaschalis, “Parametric analysis for the installation of solar dish technologies in Mediterranean regions,” Renew. Sustain. Energy Rev., vol. 14, no. 9, pp. 2772–2783, 2010.

[4] K. S. Reddy and G. Veershetty, “Viability analysis of solar parabolic dish stand-alone power plant for Indian conditions,” Appl. Energy, vol. 102, pp. 908–922, 2013.

[5] K. Lovegrove, G. Burgess, and J. Pye, “A new 500m2 paraboloidal dish solar concentrator,” Sol. Energy, vol. 85, no. 4, pp. 620–626, 2011.

[6] F. Nepveu, A. Ferriere, and F. Bataille, “Thermal model of a dish/Stirling systems,” Sol. Energy, vol. 83, no. 1, pp. 81–89, 2009.

[7] S. Y. Wu, L. Xiao, Y. Cao, and Y. R. Li, “A parabolic dish/AMTEC solar thermal power system and its performance evaluation,” Appl. Energy, vol. 87, no. 2, pp. 452–462, 2010.

[8] C. H. Cheng and H. S. Yang, “Optimization of geometrical parameters for Stirling engines based on theoretical analysis,” Appl. Energy, vol. 92, pp. 395–405, 2012.

[9] Z. Herzog, “Stirling Engines,” 2006.

[10] S. M. Sadrameli, “Mathematical models for the simulation of thermal regenerators: A state-of-the-art review,” Renewable and Sustainable Energy Reviews, vol. 58. pp. 462–476, May-2016.

[11] M. B. Ibrahim, R. C. Tew, and Jr., Stirling Convertor Regenerators, vol. 16. CRC Press, 2011.

[12] B. Kongtragool and S. Wongwises, “Thermodynamic analysis of a Stirling engine including dead volumes of hot space, cold space and regenerator,” Renew. Energy, vol. 31, no. 3, pp. 345–359, Mar. 2006.

[13] S. Alfarawi, R. Al-Dadah, and S. Mahmoud, “Enhanced thermodynamic modelling of a gamma-type Stirling engine,” Appl. Therm. Eng., vol. 106, pp. 1380–1390, Aug. 2016.

[14] MATLAB, version 7.10.0 (R2010a). Natick, Massachusetts: The MathWorks Inc., 2010.

[15] ETEC California; and EPRI, “Performance of the Vanguard solar dish-Stirling engine module,” Rockwell International Corp., Canoga Park, CA (USA). Energy Technology Engineering Center, 1986.

[16] T. Mancini, P. Heller, B. Butler, B. Osborn, W. Schiel, V. Goldberg, R. Buck, R. Diver, C. Andraka, and J. Moreno, “Dish-Stirling Systems: An Overview of Development and Status,” J. Sol. Energy Eng., vol. 125, no. 2, p. 135, 2003.

[17] K. Stone, E. Leingang, G. Rodriguez, J. Paisley, J. Nguyen, T. Mancini, and H. Nelving, “Performance of the SES/Boeing dish Stirling system,” Sol. Eng., pp. 97–104, 2001.

[18] J. B. Mayette, R. L. Davenport, and R. E. Forristall, “The Salt River Project Sundish dish-sterling system,” Sol. Eng. 2001, pp. 83–87, 2001.

[19] R. S. Moghadam, H. Sayyaadi, and H. Hosseinzade, “Sizing a solar dish Stirling micro-CHP system for residential application in diverse climatic conditions based on 3E analysis,” Energy Convers. Manag., vol. 75, pp. 348–365, 2013.

[20] A. Z. Hafez, A. Soliman, K. A. El-Metwally, and I. M. Ismail, “Solar parabolic dish Stirling engine system design, simulation, and thermal analysis,” Energy Convers. Manag., vol. 126, pp. 60–75, Oct. 2016.